Final Draft
of the original manuscript:

Witte, K.; Bodnar, W.; Schell, N.; Fulda, G.; Burkel, E.:
Phase transformations of stoichiometric mixtures of hematite and iron under FAST conditions
In: Journal of Alloys and Compounds (2017) Elsevier

DOI: 10.1016/j.jallcom.2017.07.089

Phase transformations of stoichiometric mixtures of hematite and iron under FAST conditions

Kerstin Witte[1,*], Wiktor Bodnar[1], Norbert Schell[2], Gerhard Fulda[3], Eberhard Burkel[1,**]

[1] *University of Rostock, Institute of Physics, Albert-Einstein - Str. 23, D-18059 Rostock, Germany,*

[2] *Helmholtz-Center Geesthacht, Institute of Materials Research, Max-Planck-Str. 1, D-21502 Geesthacht, Germany*

[3] *University Medicine Rostock, Medical Biology and Electron Microscopy Centre, Strempelstr. 14, D-18057 Rostock, Germany*

[*] *Corresponding author, e-mail: kerstin.witte@uni-rostock.de*

[**] *Principal corresponding author*

Abstract

Since the mechanism of the synthesis of magnetite from a stoichiometric mixture of hematite and iron is still under debate, systematic studies of the phase transformations in such powder mixture processed under field assisted sintering conditions, are presented. Phase contributions, grain sizes and stoichiometries of the sintered composites were determined using scanning electron microscopy, high energy X-ray diffraction and Mößbauer spectroscopy. It was shown that with an increasing sintering temperature an accelerated growth of magnetite can be observed, while the amount of hematite decreases. Additionally, intermediate wustite phase was observed with a maximum intensity where iron vanished from the samples. Thereofore, it was concluded that the transition from hematite - iron mixture to magnetite actually takes place in two steps. In the first step, iron reduces hematite to magnetite and oxidizes itself to wustite. In the second step, wustite enables the nucleation of magnetite and with the help of hematite it transforms into nearly pure stoichiometric magnetite at higher sintering temperatures. In composites sintered from pure hematite under the same conditions only a minor transition to highly nonstoichiometric magnetite was observed emphazising the above mentioned route of transformation.

Keywords: iron oxides; magnetite; phase transformations; nanocomposites; field assisted sintering technique (FAST)

1. Introduction

Nanostructured materials attracted a lot of attention in the last years due to their unusual chemical and physical properties which are promising for further technological development [1-3]. The properties of these nanostructured materials differ from those of normal bulk materials due to the small particle- or grain sizes which are in the nanometer regime leading to the presence of size and surface effects [1].

The rather novel field assisted sintering technique (FAST), also called spark plasma sintering (SPS), is a promising tool for the consolidation and synthesis of such nanostructured bulk materials. During FAST a pulsed directed current and a mechanical load are applied on precursor powders placed in a graphite die, leading to rapid heating of the powders [4]. Advantages of FAST are short process times and the possibility of maintaining nanostructured grains [4,5].

The preparation as well as the properties of iron oxides still attract considerable interest and attention in materials technology. Particularly, the interest in magnetic nanoparticles based on iron oxides rose drastically because of their wide range of potential applications, especially in biomedicine [2,3,6,7,8]. For nanoparticles and thin films, a broad range of interesting effects like superparamagnetism [9], giant magnetoresistance [10] or increased energy product [11] has been observed, while the behaviour of nanostructured bulk materials based on iron oxides is widely unknown. First studies on iron oxide systems already showed changes in the coercivity and the saturation magnetisation for different grain sizes [12-16].

In the family of iron oxides magnetite (Fe_3O_4) and maghemite (γ-Fe_2O_3) are the most important ferrimagnetic compounds. The stoichiometry of magnetite, which is often referred to as a solid solution of magnetite and maghemite, strongly influences the physical and

chemical properties as the reduction potential, coercivity or crystal structure of the particles [17]. Magnetite has a cubic unit cell which belongs to the space group Fd-3m and a crystal unit edge of a ~ 8.39 Å [18]. The unit cell of the stoichiometric spinel contains 32 oxygen atoms and has 8 equivalent tetrahedral and 16 equivalent octahedral sites which can be occupied by iron atoms. Magnetite contains not only trivalent but also divalent iron in the octahedral sites. The formula of Fe_3O_4 can also be presented as $(Fe^{3+})_{tetra}[Fe^{3+}+Fe^{2+}]_{octa}O_4^{2-}$ [19]. Magnetite has a wide range of oxidation states depending on the structural Fe^{2+} states, which can be discussed as the stoichiometry of magnetite ($x=Fe^{2+}/Fe^{3+}$). x=0.5 refers to the stoichiometric magnetite Fe_3O_4 and x=0 to its completely oxidised form, maghemite γ-Fe_2O_3. Maghemite is characteristic of a crystal unit edge a ~ 8.33 Å [18]. For non-stoichiometric magnetite, the structure formula can be presented as $Fe_{3-\delta}O_4$ with δ ranging from 0 to 1/3. Assuming that the vacancies □ are only present on the octahedral sites, the formula can be written as $(Fe^{3+})_{tetra}\ [Fe^{3+}_{1+2\delta}+Fe^{2+}_{1-3\delta}\square_{\delta}]_{octa}O_4^{2-}$ [17].

Furtheromre, the family of iron oxides stands out due to the great variety of possible interconversions between different phases [18]. This means that nearly every iron oxide can be transformed into another. For example, magnetite can be obtained from hematite by reduction in a reducing gas, as well as by reduction-dissolution reprecipitation in an alkaline solution [18]. Likewise, maghemite can be obtained from hematite by thermal conversion [18]. Bulk ferrimagnetic nanostructured iron oxides were mainly synthezised from maghemite. Field assisted sintering of commercially available γ-Fe_2O_3 powders with particle sizes of 8 nm and 40 nm in the temperature regime 300°C - 900°C resulted in a partial conversion of maghemtite into hematite [12-14]. It was also shown that the obtained materials were composites of multiple iron oxide phases, and that with an increasing sintering temperature the fraction of hematite phase decreased [13]. It enabled the observation of exchange bias in the large three dimensional components [14]. Moreover, pure bulk nanstructured maghemite was obtained by field assisted sintering of precipitated γ-Fe_2O_3 powder at relatively low temperatures of only 300°C - 350°C and an applied pressure of 120 MPa [15]. Other approaches of top- down methods showed that using a stoichiometric

mixture of hematite and iron in high energy ball milling can lead to pure magnetite with enhanced coercivity values [20]. Nerverthess, the obtained powder was not stable upon heating in air [20].

Considering this, it was interesting to process with FAST a stoichiometric mixture of hematite and iron in a wide temperature range. The grain sizes, the composition and the stoichiometry of magnetite all influence the overall physical properties of the resulting bulk composites. Therefore, the transformation and the evolution of particular phases in the sintered materials were investigated ex-situ. In particular, the phase contributions, the grain sizes as well as the stoichiometry were studied in dependence of the sintering temperature using scanning electron microscopy, high energy X-ray diffraction and Mößbauer spectroscopy. These results were compared with their conuterparts obtained for composites sintered only from pure hematite powder.

2. Field assisted sintering

Hematite and iron powders with mean particles size of 190(10) nm and 220(60) nm, respectively, were mixed assuming the following reaction

$$4\,Fe_2O_3 + Fe \rightarrow 3\,Fe_3O_4\,. \qquad (1)$$

Further details on the precursor powders are summarized in the supplementary. All samples were designed to have a thickness of approximately 4 mm after consolidation. The appropriate amounts of powders were weighted using a precise laboratory balance and blended in grinding jars for 20 min in order to ensure homogeneity. The obtained precursor was placed in a graphite die with an inner diameter of 40 mm. The powder was separated from the inner walls of the die and the punches by a graphite foil in order to prevent reactions with the graphite dies and to ensure an electric contact. In order to reduce radiation heat losses from the outer surface of the die, the graphite die was covered with a porous carbon felt. The application of a carbon felt also reduces possible gradients of temperature in the sample [21,22] and ensures maximal possible in-plane homogeneity of the obtained sample.

The sintering procedure was performed in Tycho Sinterlab Rostock using a HP D125 unit from FCT Systeme GmbH Rauenstein, Germany. A series of samples was sintered at different temperatures ranging from 600°C to 950°C with a step of 50 K.

Fig. 1 presents exemplary real-time data of the temperature (solid line) and the plunger displacement (dashed line), corresponding to the densification of material [4], during the sintering procedure. In the case of the hematite and iron precursor, the plunger displacement cannot lead to further conclusions due to occuring phase transition into magnetite. The process was divided into four characteristic phases marked in Fig. 1 with vertical dashed lines.

In the first phase, the sintering chamber was evacuated to approximately 1 mbar. Next, the pressure and the temperature were increased to 28 MPa and 400°C, respectively. Here, it is worth to mention that due to technical limitations the heating process below 400°C was controlled by a thermocouple mounted in the graphite die and above 400°C by an optical pyrometer focused on a surface approximately 4 mm away from the sample, in a hole drilled in the upper graphite punch. In the second phase, the temperature was raised to 900°C and the pressure to 50 MPa. In all cases, this segment time was kept constant (5 min) in order to exclude its influence on the phase transformations and the grain growth. Next, the temperature and the pressure were held constant for another 5 min. Finally, the pressure was released and the pulsed directed current was turned off.

The post-sintered discs were cleaned from the protective graphite foil and broken. Pieces from the middle of each disc were used to prepare samples for further investigations with scanning electron microscopy, high energy X-ray diffraction and Mößbauer spectroscopy.

3. Experimental details

3.1 Scanning electron microscopy

The microstructure of the sintered iron oxide composites was investigated using Zeiss DSM 960A scanning electron microscope (SEM). The fracture surfaces of the composites were

additionally covered by a thin layer of carbon using a Leica EM SCD500 sputter coater in order to ensure conductivity. The SEM images of the fracture surfaces are presented in Fig. 2. With an increasing sintering temperature an increase in the mean grain size can be observed. Furthermore, the interconnectivity between the grains increases leading to smoother surfaces at the breaking edges.

3.2 High energy X-ray diffraction

Synchrotron radiation is well suited to investigate complex crystal structures and phase compositions of bulk materials because of the high penetration power, high photon flux and excellent brilliance of modern synchrotron sources. Moreover, synchrotron radiation fulfills the need for high resolution, imposed by the nature of composites containing finely dispersed phases with less intense diffraction patterns.

High energy X-ray diffraction studies were performed at the High Energy Material Science (HEMS) beamline P07 located at the high brilliance synchrotron radiation storage ring PETRA III, DESY Hamburg, Germany. The basic design parameters of the storage ring are an energy of 6 GeV and a current of 100 mA. The source of X-rays for HEMS is a 2 m long standard PETRA undulator. Investigations were performed in the test facility EH1 using an indirectly water-cooled single bounce monochromator with a Si(220) Laue single-crystal leading to monochromatic synchrotron radiation with a wavelength $\lambda = 0.1424$ Å [23,24]. The experiments were carried out in transmission Debye-Scherrer geometry with a sample to detector distance of 1200 mm. The diffraction patterns were collected with a Perkin Elmer image plate detector, characteristic of a resolution of 2048 x 2048 pixels and a pixel size of 200 µm. The calibration of the experimental setup was performed using a standard Al_2O_3 flat-plate.

The collected diffraction patterns were integrated in 5° steps and processed applying Rietveld refinement procedure [25] combined with the Fourier analysis as implemented in the MAUD code [26,27]. Fig. 3 shows the experimental and the calculated diffractograms, as well

as the differential patterns. Additionally, the Bragg reflexes of particular phases, namely magnetite, hematite, iron and wustite, are indicated.

Due to the changing volume fractions of the contributing phases, the peaks ascribed to hematite decrease while those corresponding to magnetite increase significantly with increasing sintering temperature. Moreover, a slight decrease of the half width of all diffraction peaks can be observed. The presence of small fractions of wustite and iron was also confirmed by the Rietveld refinement procedure.

3.3 Mößbauer spectroscopy

^{57}Fe Mößbauer spectroscopy investigations were performed in transmission geometry at room temperature. The γ-ray source was ^{57}Co embedded in a Rh matrix. The source was mounted in a FAST Comtec Mößbauer drive unit working in constant acceleration mode. The spectra were collected with a scintillation counter and the spectrometer was calibrated using standard ARMCO foil. All samples were prepared following the assumptions of the thin absorber approximation [28,29].

Based on the high energy X-ray diffraction data, the collected Mößbauer spectra were fitted assuming a five component system. Antiferromagnetic hematite [18,30] and ferromagnetic iron show a single sextet at room temperature. Magnetite shows two sextets which are related to different positions (A- and B-sites) in the crystal lattice [18,30,31]. The A-sites are occupied only by Fe^{3+}-ions while the B-sites can be occupied by both Fe^{2+}- or Fe^{3+}-ions. Furthermore, a fast electron hopping above the Verwey transition temperature takes place on the B-sites [32]. Therefore, only one sextet corresponding to a mixed valence state 2.5+ of Fe can be seen on the B-sites at room temperature. Wustite which is paramagnetic at room temperature is represented by a doublet [18].

Fig. 4 presents the transmission Mößbauer spectra and the fitted patterns of the composites from hematite and iron precursor powders processed by FAST at different temperatures. The evolution of the Mößbauer spectra clearly indicates phase transitions occuring at different

sintering temperatures. The intensities of lines corresponding to hematite decrease while of the ones corresponding to magnetite increase with increasing sintering temperature. The fitting procedure also confirmed the presence of wustite and iron in the tested composites.

4. Results and discussion

Since the mechanism of the synthesis of magnetite using hematite and iron as precursors is not clear yet, the transformation of a stoichiometric mixture of hematite and iron into magnetite under FAST conditions was systematically studied. Materials were sintered in vacuum at temperatures ranging from 600°C to 950°C in 50 K steps with 5 min holding time at the elevated temperatures. Uniaxial pressure of 50 MPa was applied. Mechanicaly stable bulk composites were obtained under these sintering conditions. Here, it is worth to mention that the heating rate in each process was adjusted to ensure a constant overall process time allowing for a direct comparison of the post-sintered composites.

4.1 Composition

Two main phases, namely hematite and magnetite, were detected by means of X-ray diffraction and Mößbauer spectroscopy in the composites from hematite and iron precursor powders processed by FAST. Moreover, the presence of iron and wustite was also confirmed. Fig. 5A shows the volume fractions of magnetite, hematite, iron and wustite, determined by high energy X-ray diffraction. The relative intensities of the contributing phases derived by Mößbauer spectroscopy are presented in Fig. 5B. The corresponding values of the volume fraction and relative area are presented in the supplementary in Tab. S2 and S3, respectively. For both volume fraction and relative area, similar behaviour of the four phases can be observed. Volume fractions of iron and hematite are reduced and the one of magnetite rises with the increasing sintering temperature. The volume fraction of wustite shows an interesting behaviour. First, it rises and then it reaches a maximum whereas the iron phase disappears at approximately 750°C and vanishes at high sintering temperatures.

An additional presence of wustite in the investigated composites leads to the conclusion that the assumed transition of the stoichiometric mixture of hematite and iron to magnetite does not take place in a single step but in a sequential two step procedure according to the following formulae:

$$2\,Fe_2O_3 + Fe \rightarrow Fe_3O_4 + 2\,FeO \quad (2)$$

$$Fe_2O_3 + FeO \rightarrow Fe_3O_4\ . \quad (3)$$

In the first step, hematite and iron form magnetite and wustite, and in the second step hematite and wustite react to magnetite. Eventually, nearly pure magnetite is present for high sintering temperatures.

For a comparison, pure hematite powder was processed with field assisted sintering in the same temperature regime. The sintered samples were also investigated by Mößbauer spectroscopy and high energy X-ray diffraction. Fig. 6 shows relative intensities of the contributing phases, namely hematite and magnetite, derived by Mößbauer spectroscopy. Additionally, two exemplary transmission Mößbauer spectra are presented as an insert. From Fig. 6 it is clear that hematite cannot completely reduce itself to magnetite under the applied conditions. Only a small fraction of magnetite is to be found in samples sintered at higher temperatures. The largest amount of magnetite, 7.1(5)%, of all samples sintered from pure hematite can be found in the composite processed at 950°C. These observations leed to the conclusion that the presence of iron is necessary for the reduction of hematite to magnetite under FAST conditions, confirming the transformation described with Eq. (2) and Eq. (3).

The synthesis of magnetite from a stoichiometric mixture of hematite and iron was already performed by ball-milling in an inert atmosphere [20]. It was pointed out that the role of the iron in this transition is not clear [20]. Hematite forms magnetite at temperatures around 350°C to 500°C and magnetite forms maghemite at temperatures around 250°C to 350°C [33]. Moreover, it was found that hematite forms wustite in a hydrogen atmosphere at temperatures below 570°C [34]. In the case of the stoichiometric mixture of hematite and iron

FAST-sintered in vacuum, iron reduces the hematite to magnetite while oxidising to wustite. Furthermore, wustite is thermodynamically unstable below 570°C and it exhibits strong deviations from stoichiometry [35]. With this nonstoichiometric structure, wustite enables the nucleation of magnetite [35]. Finally, wustite forming magnetite nuclei and hematite form nearly pure magnetite at higher sintering temperatures.

4.2 Structural properties of magnetite

Fig. 7 shows the crystal unit edge a, as well as the mean crystallite size d_c and the grain size d_g of magnetite in the composites from hematite and iron precursors sintered at different temperatures. The crystal unit edges and the crystallite sizes were derived by the Rietveld refinement procedure, while the grain sizes were determined basing on SEM images. The corresponding values are collected in Tab. S4 in the supplementary.

The crystal unit edge of magnetite is constant through the whole series of samples with a slight tendency to decrease at higher temperatures. Both mean grain and crystallite sizes exhibit similar behaviours i.e. they are approximately constant up to 850°C whereas at higher sintering temperatures an abnormal growth begins. The grain and the crystallite growths can be described with exponential functions $d_g = [243.37+0.000397 \cdot \exp(T_{sinter}/81.43/K)] \cdot nm$ and $d_c=[87.94+0.00374 \cdot \exp(T_{sinter}/92.90/K)] \cdot nm$, respectively.

Furthermore, the mean crystallite sizes determined by Rietveld refinement show the same behaviour as the mean grain sizes. This leads to the conclusion that the determined grains are actually single crystals. An exponential grain growth with increasing sintering temperature was observed in the sintered samples. This observation is in agreement with the description of grain growth depending on the reaction rate which is an exponential function of the sintering temperature [36].

4.3 Hyperfine parameters and stoichiometry of magnetite

The hyperfine interaction parameters, namely the isomer shift IS, the magnetic hyperfine field $\mu_0 H_{hf}$ and the quadrupole interaction parameter QS of magnetite phase for A- and B-sites,

are presented in Fig. 8. The hyperfine interaction parameters for all contributing phases are listed in Tab. S3 in the supplementary.

The relative intensities of the contributing phases, namely hematite, iron, magnetite and wustite, stay in good agreement with their counterparts, volume fractions, determined by X-ray diffraction. For lower sintering temperatures the hyperfine interaction parameters of magnetite differ from typical bulk values. The changes of the hyperfine parameters are mainly to be seen for A-sites of the crystal lattice of magnetite. The hyperfine interaction parameters of magnetite B-sites show only small deviations from being constant. The changes of the hyperfine parameters can be caused by the fitting procedure due to the changing ratio of hematite to magnetite influencing mainly magnetite A-sites. These changes are neither a result of grain size nor interaction effects. Presumably, they are a result of the fitting procedure due to a large amount of hematite present in the samples sintered at lower temperatures.

The stoichiometry of magnetite in the investigated series of composites, determined from the Mößbauer spectra using the relative intensities of A- and B-sites, can be identified with the number of vacancies per formula unit. Fig. 9 shows the number of vacancies δ per formula unit of the magnetite phase in the composites from hematite and iron precursors sintered at different temperatures. The values of δ are also collected in Tab. S4 in the supplementary. It was found that δ is approximately constant through the whole series with a mean value of 0.018(5). This relatively small value means that magnetite synthesized during the FAST process is nearly stoichiometric with the stoichiometric formula $Fe_{2.982}O_4$.

On the contrary, the magnetite present in the composites sintered from pure hematite precursor shows a highly nonstoichiometric character. The number of vacancies δ ranged from 0.32(2) at lower sintering temperatures to 0.25(2) at higher temperatures.

For δ = 0.32, the stoichiometry of the cubic spinell is $Fe_{2.68}O_4$ which corresponds to nearly pure maghemite. At higher sintering temperatures the stoichiometry changes slightly to $Fe_{2.75}O_4$ meaning that the direct reduction of hematite to magnetite is highly unlikely under

the investigated conditions. The presence and the oxidation of iron to wustite are necessary for building nucleation points of pure stoichiometric magnetite.

5. Conclusions

A stoichiometric mixture of hematite and iron powder were consolidated into stable bulk composites using field assisted sintering in the temperature range of 600°C to 950°C. It was found that during the FAST process, iron reduces hematite to magnetite while oxidizing to wustite. With its nonstoichiometric structure wustite enables the nucleation of magnetite and at higher sintering temperatures, wustite and hematite transform to nearly pure stoichiometric magnetite with the formula $Fe_{2.982}O_4$. The crystal unit edge and the stoichiometry of magnetite stay approximately constant for all sintering temperatures. The grain and crystallite sizes both show similar exponential growth with increasing sintering temperature. Morover, pure hematite powder was processed by FAST in the same temperature regime. Here, only a minor transition to highly nonstoichiometric magnetite was observed. Therefore, the presented *ex-situ* studies of the phase transitions in a stoichiometric mixture of hematite and iron processed under FAST conditions clarifyed the role of iron in this route for the synthesis of stoichiometric magnetite.

References

[1] G.C. Hadjipanayis, Nanophase hard magnets, Journal of Magnetism and Magnetic Materials 200 (1999) 373.

[2] M. Colombo, S. Carregal-Romero, M.F. Casula, L. Gutierrez, M.P. Morales, I.B. Böhm, J.T. Heverhagen, D. Rosperi, W.J. Parak, Biological applications of magnetic nanoparticles, Chemical Society Reviews 41 (2012) 4306.

[3] Q.A. Pankhurst, The magnetism of fine particle iron oxides and oxyhydroxides in applied fields, Hyperfine Interactions 90 (1994) 201.

[4] J E Garay, Current-activated, pressure-assisted densification of materials, Annual Review of Materials Research 40 (2010) 445.

[5] R. Orru, R. Licheri, A.M. Locci, A. Cincotti, G. Cao, Consolidation/synthesis of materials by electric current activated/assisted sintering, Materials Science and Engineering: R: Reports 63 (2009) 127.

[6] P. Tartaj, M.P. Morales, S. Veintemillas-Verdaguer, T. Gonzalez-Carreno, C.J. Serna, The preparation of magnetic nanoparticles for applications in biomedicine, Journal of Applied Physics D: Applied Physics 36 (2003) R182.

[7] K. Witte, K. Porath, E. Burkel, Magnetic nanoparticles and their potential for contrast enhancement in magnetic resonance imaging, Journal of Spintronics and Magnetic Nanomaterials 1 (2012) 40.

[8] K. Witte, C. Grüttner, W. Bodnar, E. Burkel, Magnetic nanoparticles for biomedical applications, in Encyclopedia of Nanotechnology, B. Bhushan (ed.), Springer Science+Business Media Dordrecht 2015.

[9] C.P. Bean, J.D. Livingston, Superparamagnetism, Journal of Applied Physics 30 (1959) 120.

[10] A. Fert, P. Grünberg, A. Barthelemy, F. Petroff, W. Zinn, Layered magnetic structures: interlayer exchange coupling and giant magnetoresistance, Journal of Magnetism and Magnetic Materials 140-144 (1995) 1.

[11] R. Skomski, J.M.D. Coey, Giant energy product in nanostructured two-phase magnets, Physical Review B 48 (1993) 15812.

[12] J.R. Morales, J.E. Garay, M. Biasini, W.P. Beyermann, Magnetic characterization of bulk nanostructured iron oxides, Applied Physics Letters 93 (2008) 022511.

[13] J.E. Alaniz, J.R. Morales, J.E. Garay, The current activated pressure assisted densification technique for producing nanocrystalline materials, The Member Journal of The Minerals, Metals and Materials Society (2010) 58.

[14] J.R. Morales, S. Tanju, W.P. Beyermann, J.E. Garay, Exchange bias in large three dimensional iron oxide nanocomposites, Applied Physics Letters 96 (2010) 013102.

[15] P. Saravanan, J.-H. Hsu, D. Sivaprahasam, S.V. Kamat, Structural and magnetic properties of γ-Fe_2O_3 nanostructured compacts process by spark plasma sintering, Journal of Magnetism and Magnetic Materials 346 (2013) 175.

[16] C. Fei, Y. Zhang, Z. Yang, Y. Liu, R.W. Xiong, J. Shi, X. Ruand, Synthesis and magnetic properties of hard magnetic ($CoFe_2O_4$)-soft magnetic (Fe_3O_4) nano-composite ceramics by SPS technology, Journal of Magnetism and Magnetic Materials 323 (2011) 1811.

[17] C.A. Gorski, M.M. Scherer, Determination of nanoparticulate magnetite stoichiometry by Mössbauer spectroscopy, acidic dissolution, and powder X-ray diffraction: A critical review, American Mineralogist 95 (2010) 1017.

[18] R.M. Cornell, U. Schwertmann, The iron oxides - structure, properties, reactions, occurence and uses, VCH: New York 1996.

[19] I. Mitov, Z. Cherkezova-Zheleva, V. Mitrov, Comparative study of the mechanochemical activation of magnetite (Fe3O4) and maghemite γ-Fe_2O_3), Physica status solidi A 161 (1997) 475.

[20] E. Petrovsky, M.D. Alcala, J.M. Criado, T. Grygar, A. Kapicka, J. Subrt, Magnetic properties of magnetite prepared by balball-mill of hematite and iron, Journal of Magnetism and Magnetic Materials 210 (2000) 257.

[21] U. Anselmi-Tamburini, S. Gennari, J.E. Garay, Z.A. Munir, Fundamental investigations on the spark plasma sintering/synthesis process: II. Modeling of current and temperature distributions, Materials Science and Engineering: A 394 (2005) 139.

[22] X. Wang, S.R. Casolco, G. Xu, J.E. Garay, Finite element modeling of electric current-activated sintering: the effect of coupled electrical potential, temperature and stress, Acta Materialia 55 (2007) 3611.

[23] N. Schell, A. King, F. Beckmann, H.U. Ruhnau, R. Kirchhof, R. Kiehn, M. Müller, A. Schreyer, The High Energy Materials Science Beamline at PETRA III, AIP Conference Proceeding 1234 (2010) 391.

[24] N. Schell, A. King, F. Beckmann, T. Fischer, M. Müller, A. Schreyer, The High Energy Materials Science Beamline at PETRA III, Material Science Forum 772 (2014) 57.

[25] H.M. Rietveld, A profile refinement method for nuclear and magnetic structures, Journal of Applied Crystallography 2 (1969) 65.

[26] L. Lutterotti, M. Bortolotti, G. Ischia, I. Lonardelli, H.R. Wenk, Rietveld texture analysis from diffraction images, Zeitschrift für Kristallographie Supplements 2007 (2007) 125.

[27] L. Lutterotti, S. Matthies, H.R. Wenk, A.J. Schultz, J. Richardson, Combined texture and structure analysis of deformed limestone from time-of-flight neutron diffraction spectra, Journal of Applied Physics 81 (1997) 594.

[28] Y.L. Chen, D.P. Yang, Mössbauer effect in lattice dynamics - experimental techniques and applications, Wiley-VHC 2007.

[29] D. Barb, Grundlagen und Anwendungen der Mössbauerspektroskopie, Akademie-Verlag Berlin 1980.

[30] E. Murad, Magnetic properties of microcrystalline iron(III) oxides and related materials as reflected in their Mössbauer spectra, Physics and chemistry of minerals 23 (1996) 248.

[31] R.E. Vandenberghe, C.A. Barrero, G.M. Da Costa, E. Van San, E. De Grave, Mössbauer characterization of iron oxides and (oxy)hydroxides: the present state of the art, Hyperfine Interactions 126 (2000) 247.

[32] E.J.W. Verwey, P.W. Haayman, Electronic conductivity and transition point of magnetite ("Fe_3O_4"), Physica 8 (1941) 979.

[33] W.A. Kaczmarek, B.W. Ninham, Preparation of Fe_3O_4 and γ-Fe_2O_3 powders by magnetochemical activation of hematite, IEEE Transactions on Magnetics 30 (1994) 732.

[34] V.P. Romanov, L.F. Checherskaya, P.A. Tatsienko, Peculiarities of wustite formed below 570°C, Physica status solidi A 15 (1973) 721.

[35] Z. Inglot, D. Wiarda, K.P. Lieb, T. Wenzel, M. Uhrmacher, Defects in $Fe_{1-x}O$ and the $Fe_{1-x}O \rightarrow Fe_3O_4$ phase transition studied by the perturbed angular correlation method, Journal of Physics: Condensed Matter 3 (1991) 4569.

[36] R.H.R. Castro, K. van Benthem, Sintering; Mechanism of convention, nanodensification and field assisted process, Springer Verlag Berlin Heidelberg 2013.

Figures and figure captions

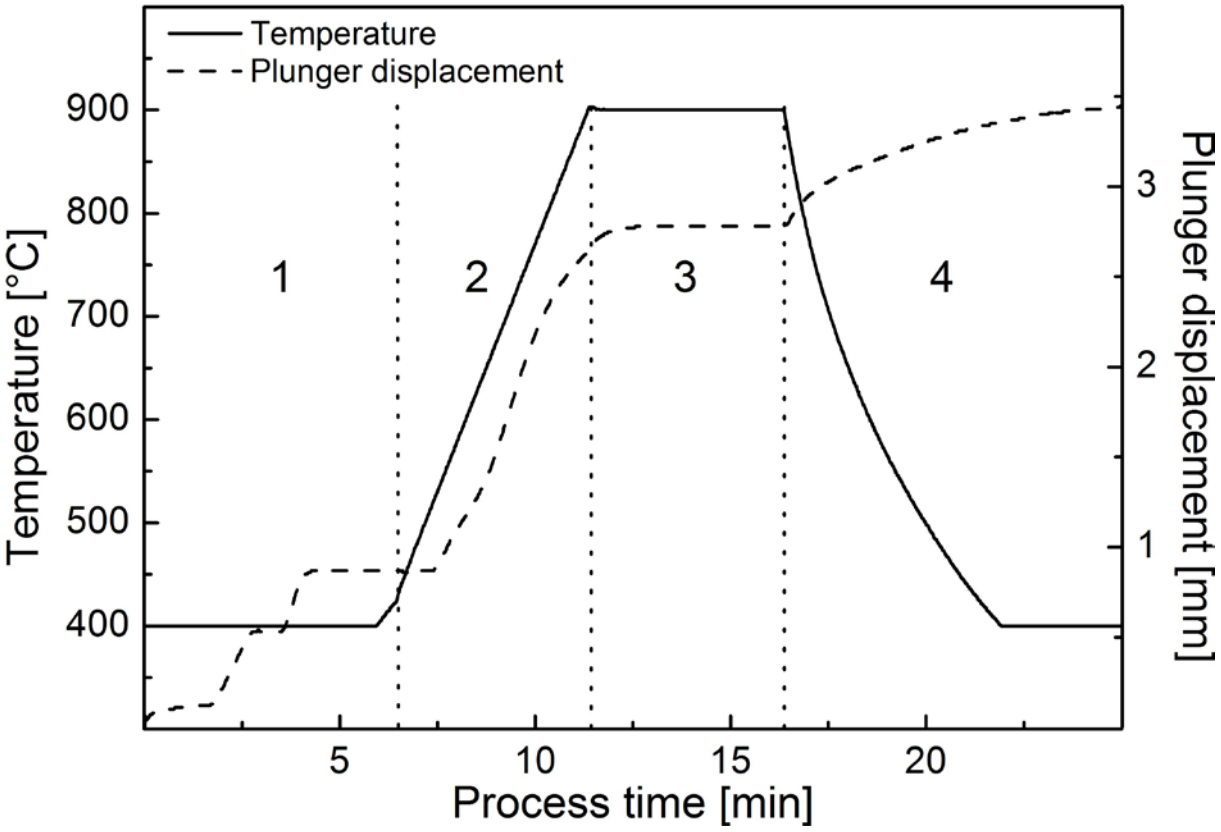

Fig. 1: Temperature and plunger displacement versus sintering time of hematite and iron precursor. Four characteristic phases of the sintering process, described in detail in text, are marked with vertical dotted lines.

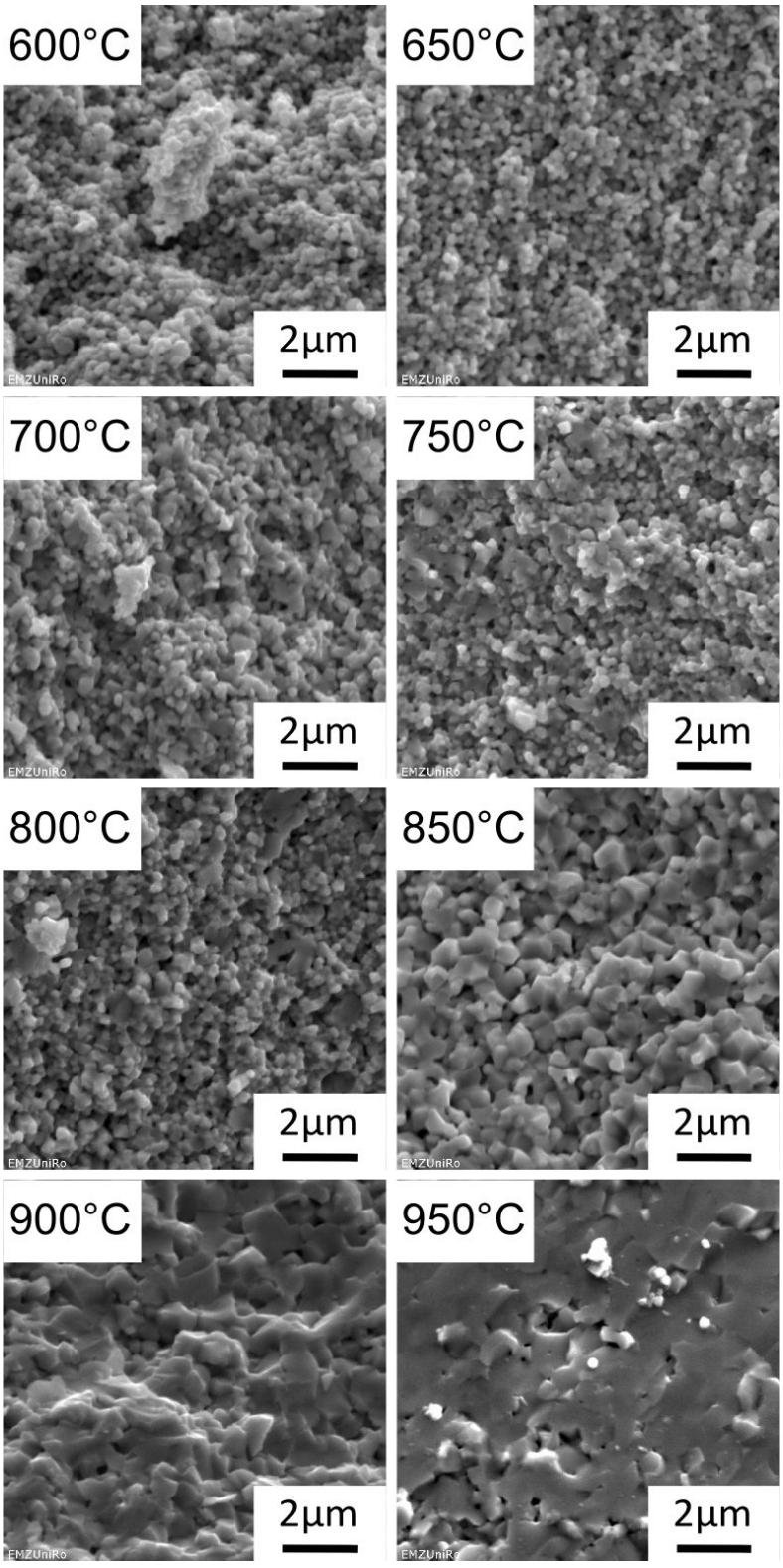

Fig. 2: SEM images of fracture surface of the composites from hematite and iron precursor powders processed by FAST at different temperatures.

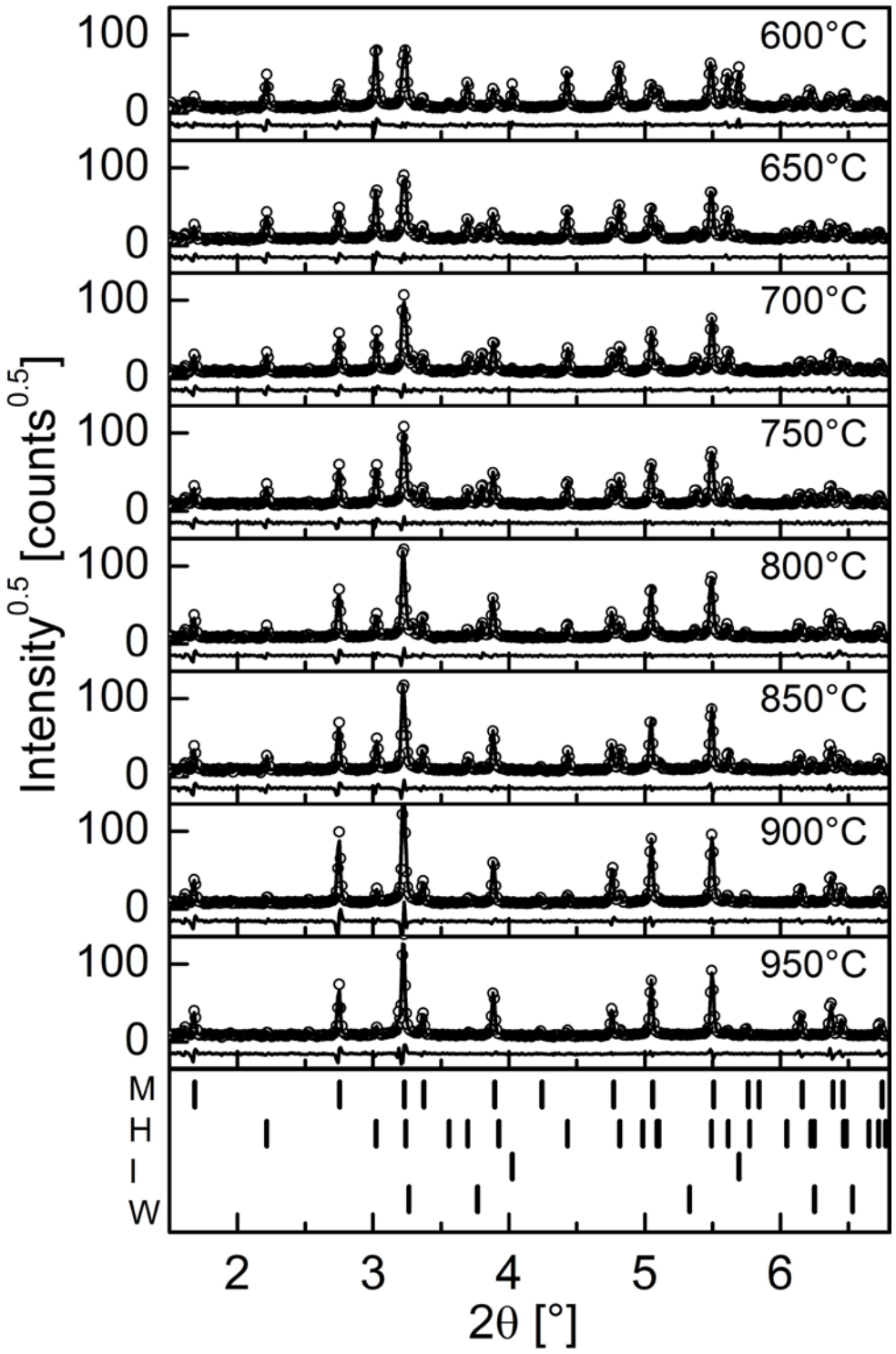

Fig. 3: High energy X-ray diffractograms of the composites from hematite and iron precursor powders processed by FAST at different temperatures. Experimental diffractogram - dots, fitted pattern - solid line. Additionally, the differential pattern is added below each diffractogram. Vertical bars represent Bragg positions of magnetite (M), hematite (H), iron (I) and wustite (W).

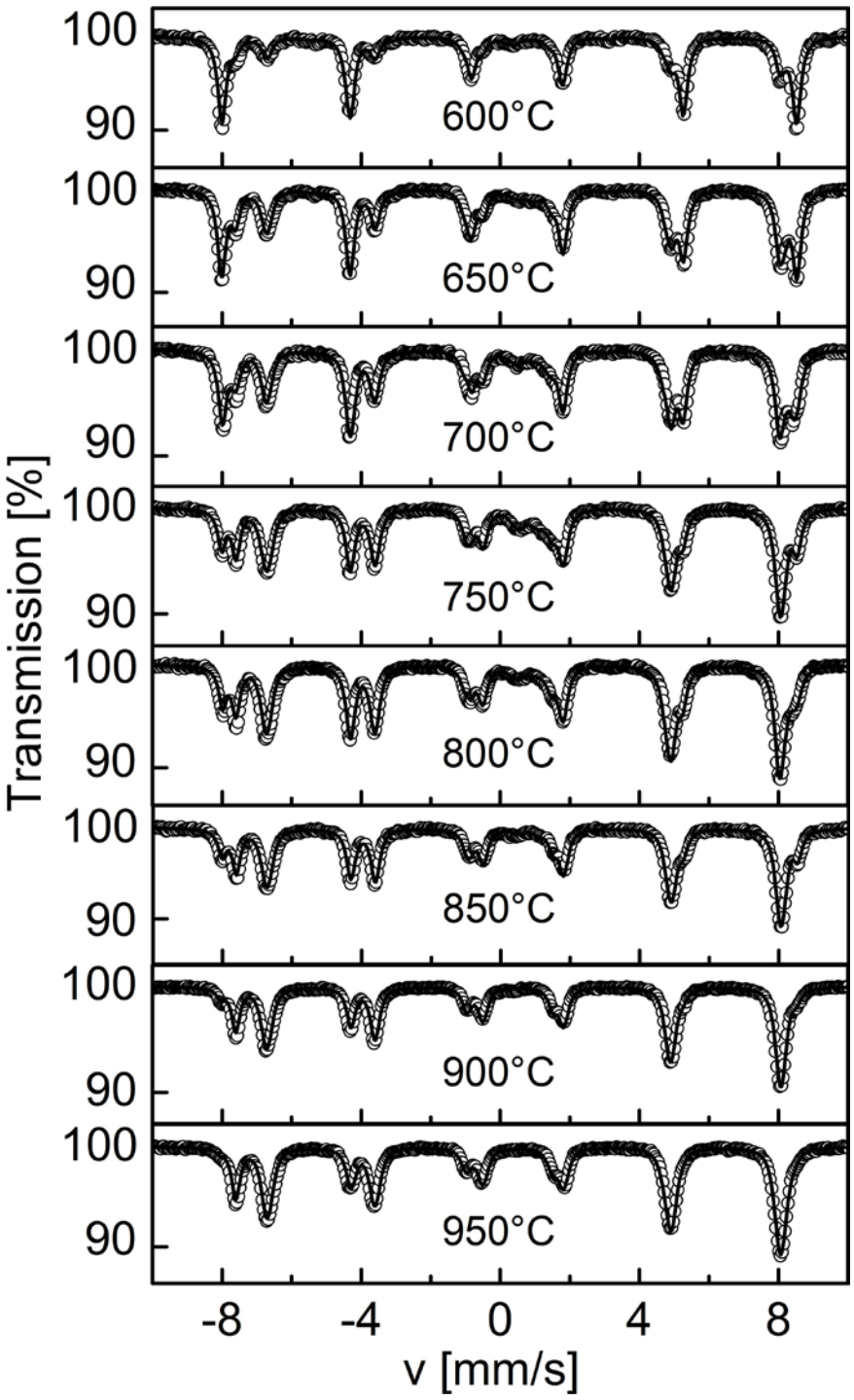

Fig. 4: Transmission Mößbauer spectra of the composites from hematite and iron precursor powders processed by FAST at different temperatures. Experimental data - dots, fitted pattern - solid line.

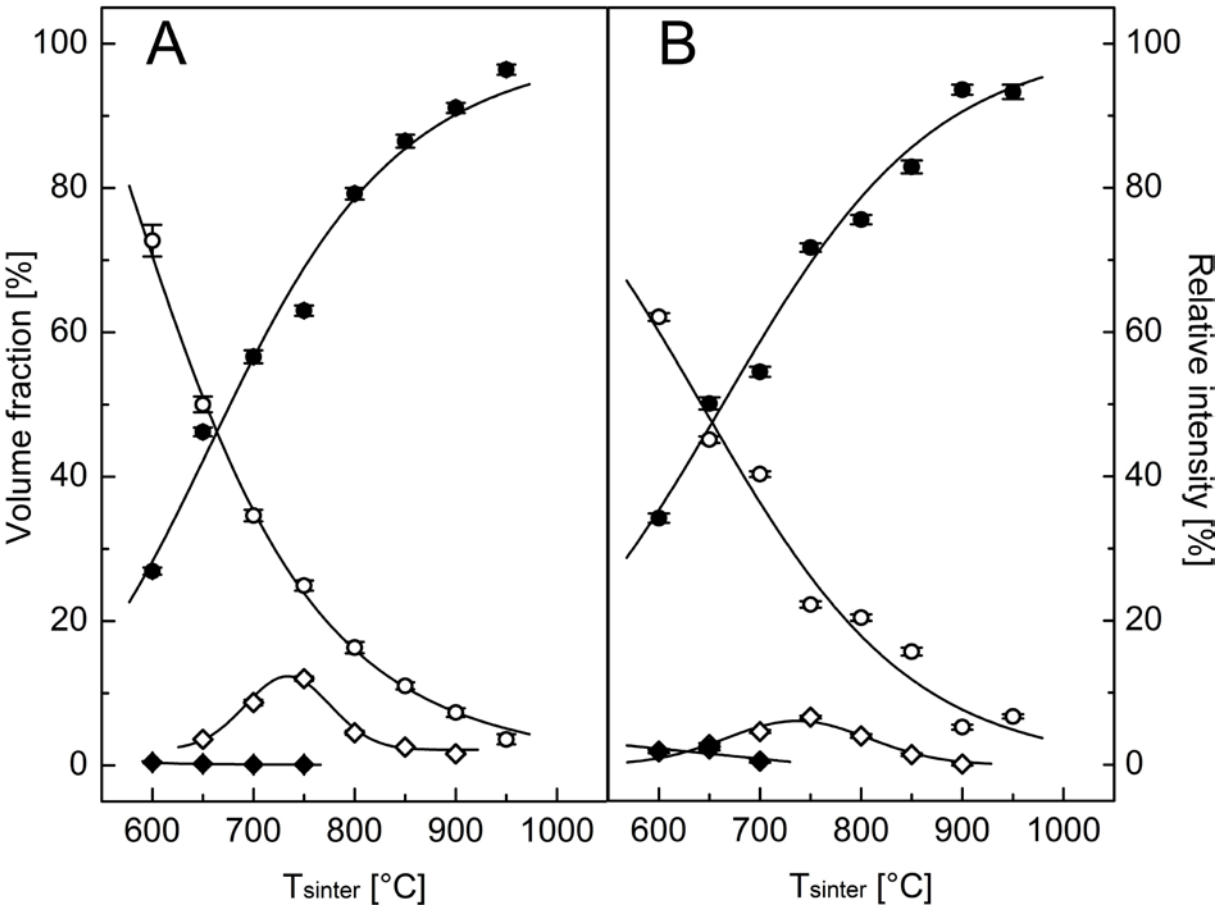

Fig. 5: Volume fractions determined by high energy X-ray diffraction (A) and the relative intensities derived by Mößbauer spectroscopy (B) of the contributing phases in dependence of the sintering temperature of the composites from hematite and iron precursor powders processed by FAST. Magnetite - black dots, hematite - open dots, iron - black diamonds and wustite - open diamonds.

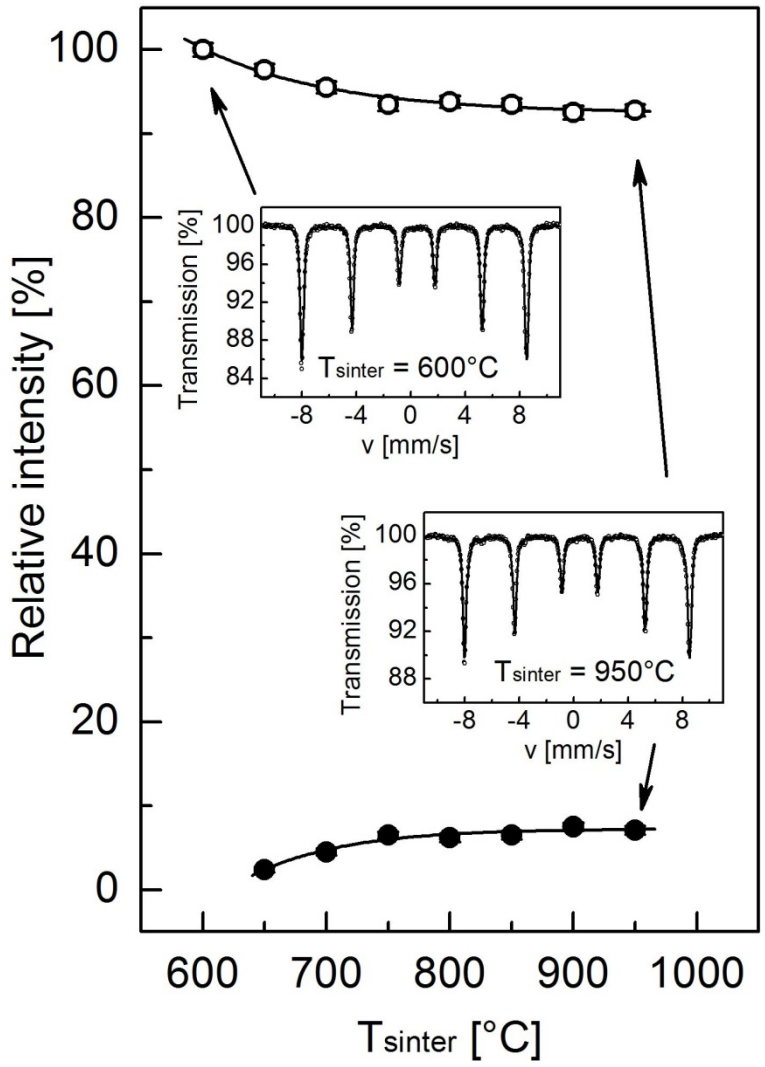

Fig. 6: Relative intensities derived by Mößbauer spectroscopy of the contributing phases in composites FAST sintered from pure hematite precursor powder in dependence of the sintering temperature. Magnetite - black dots, hematite - open dots. Additionally, two exemplary transmission Mößbauer spectra of the composites sintered at 600°C and 950°C are presented. Experimental data – dots, fit – solid line.

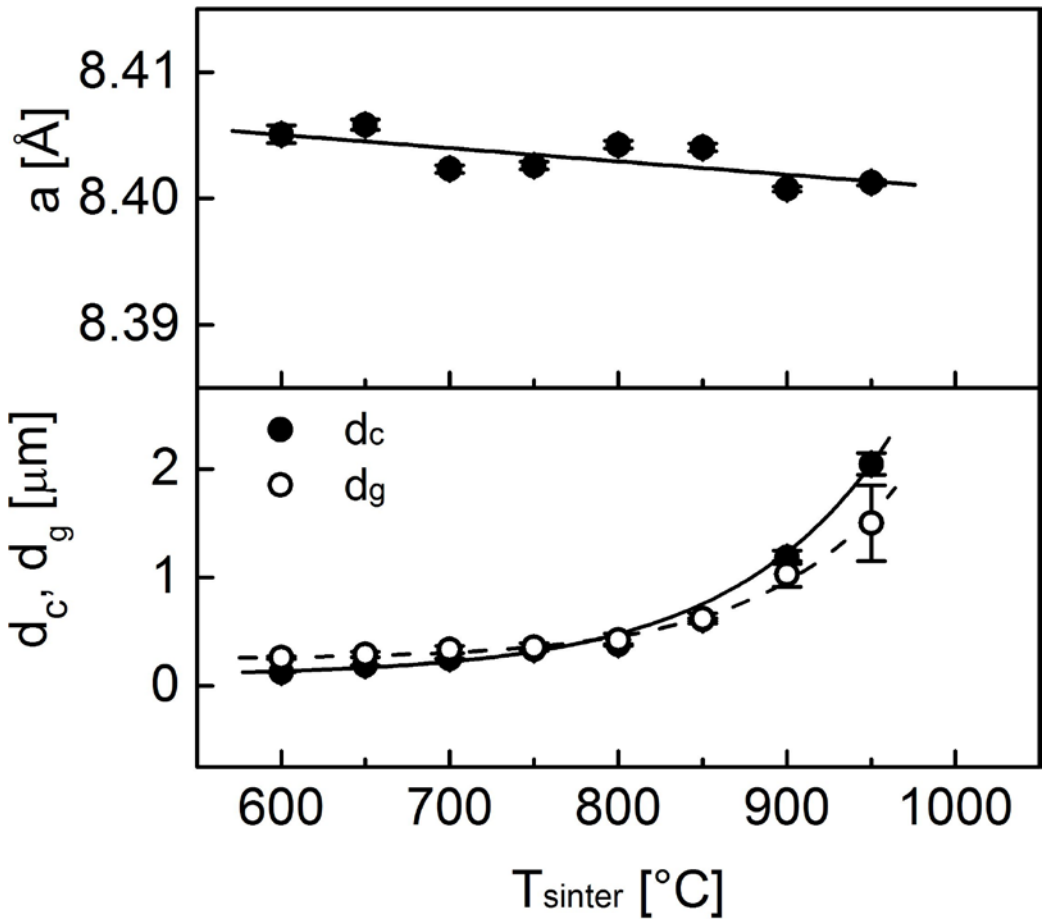

Fig. 7: Crystal unit edge (top), mean crystallite and grain size (bottom, black and open dots, respectively) of magnetite phase in the composites from hematite and iron precursor powders processed by FAST as a dependence of the sintering temperature.

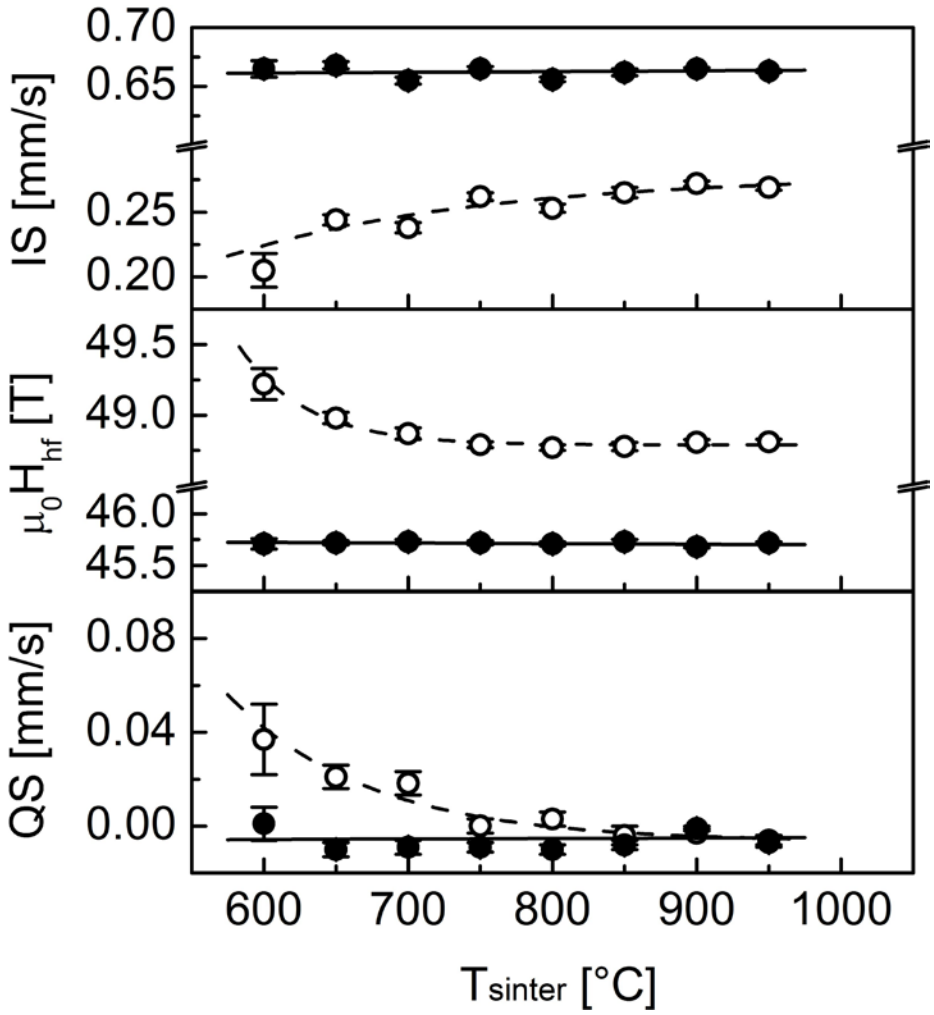

Fig. 8: Hyperfine interaction parameters: the isomer shift IS, the magnetic hyperfine field $\mu_0 H_{hf}$ and the quadrupole interaction parameter QS of magnetite phase (A-sites - open dots, B-sites - black dots) in composites processed by FAST in dependence of the sintering temperature.

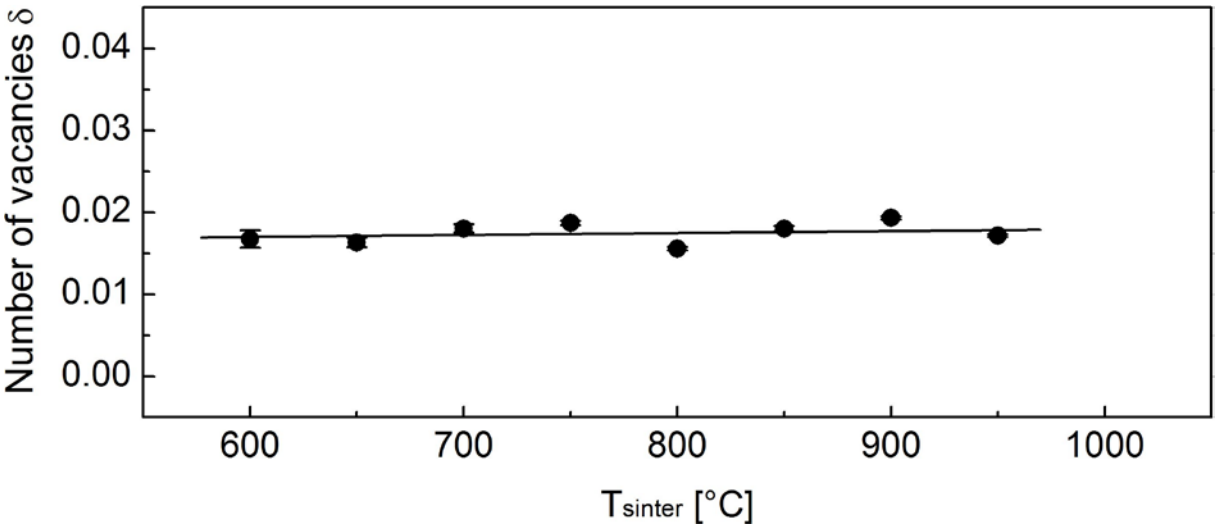

Fig. 9: Number of vacancies per formula unit of magnetite phase in the composites from hematite and iron precursor powders processed by FAST as a dependence of the sintering temperature.